A DISCONTINUOUS GALERKIN APPROACH FOR THE RADIATIVE TRANSFER APPROXIMATION OF HIGH-FREQUENCY WAVE ENERGY IN COMPLEX MEDIA

David J. Chappell[1], Robert J. Lockett[1]

[1]*Department of Physical Sciences, Nottingham Trent University, UK*

Abstract

The accurate prediction of high-frequency wave behaviour is essential for engineering applications related to noise and vibration control, but traditional finite- and boundary-element approaches typically become computationally impractical at these frequencies. We will present a transport-based framework for high frequency waves, formulated using the stationary Radiative Transfer Equation (RTE) in complex media such as piecewise homogeneous acoustic cavities and multi-plate configurations attached at line joints. Building on earlier developments in high-frequency wave energy modelling -most notably Dynamical Energy Analysis (DEA)- we retain DEA's improved fidelity and applicability over Statistical Energy Analysis. Furthermore, the RTE is spatially discretised using a discontinuous Galerkin scheme that can be implemented efficiently for any polynomial degree basis by making use of analytic integration techniques based on Stokes' theorem. Our method supports general finite element–style unstructured meshes with arbitrary polygonal elements and delivers competitive computation times suitable for large-scale applications.

Keywords: *high-frequency waves, dynamical energy analysis, radiative transfer equation, discontinuous Galerkin*

1. Introduction

High-frequency wave phenomena arise in a wide range of noise and vibration problems [1]–[3], and occur whenever the wavelength is significantly smaller than the characteristic length scales of a vibrating structure. This provides challenges in complex structures where the requirement to adequately resolve the rapid wave oscillations, as well as the complex geometric features, can lead to very large and computationally costly numerical schemes as the frequency is increased [4]–[6]. Two established high-frequency approaches are Statistical Energy Analysis (SEA), which is efficient for large systems but relies on diffuse-field and local-equilibrium assumptions [7]–[9], and ray tracing, which retains directional information but can become expensive in highly reverberant systems [10], [11]. Dynamical Energy Analysis (DEA) improves upon SEA by transporting directional energy densities on subsystem boundaries and retaining information about the underlying ray dynamics [5], [12].

Here, we introduce a new method by formulating acoustic or vibrational energy transport directly using the stationary RTE without scattering. The RTE is discretised using a discontinuous Galerkin (DG) method in space and a discrete ordinates (DO) approximation in direction, giving an element-based framework for ray (or energy) density transport on unstructured meshes. In this work, we introduce the governing RTE and its DG–DO discretisation, extend the formulation to polygonal meshes of structures comprising of plates and curved shells, and outline the treatment of multi-material interfaces and plate junctions through reflection, transmission and mode-conversion conditions in the DG flux. Preliminary validation results are then presented.

2. Problem Formulation

Let $\Omega \subset \mathbb{R}^3$ be a bounded polyhedral surface with boundary $\Gamma = \partial\Omega$, represented locally on each planar face by coordinates $\boldsymbol{x} = (x, y)$. Although embedded in three-dimensional space, wave energy is assumed to propagate tangentially along each two-dimensional surface with the propagation direction denoted by $\hat{\boldsymbol{s}}(\theta)$, where $\theta \in [-\pi, \pi)$ parametrises the local tangent-plane unit circle. For a wave mode $q \in \{B, L, S\}$, denoting bending, longitudinal and shear waves respectively, the radiance $u^q(\boldsymbol{x}, \hat{\boldsymbol{s}})$ represents the high-frequency wave energy density at $\boldsymbol{x} \in \Omega$ travelling in direction $\hat{\boldsymbol{s}}(\theta)$ and $\mu^q(\boldsymbol{x})$ represents the damping coefficient

Corresponding author: *david.chappell@ntu.ac.uk.*

for each mode. Simpler single mode acoustic wave propagation may also be modelled in an analogous manner without the need for the wave mode index q. For simplicity, throughout this work $u(\boldsymbol{x}, \hat{\boldsymbol{s}})$ and $\mu(\boldsymbol{x})$ may be interpreted as the wave energy density and damping coefficient, respectively, associated with either acoustic waves or any one of the three plate-wave modes. The coupling between these plate-wave modal components will be introduced later via interface scattering matrices, or simply via Fresnel equations for the acoustic case.

The ray (or energy) density u is characterised by the scattering free stationary RTE, given by

$$\hat{\boldsymbol{s}}(\theta) \cdot \nabla u(\boldsymbol{x}, \hat{\boldsymbol{s}}) + \mu(\boldsymbol{x})\, u(\boldsymbol{x}, \hat{\boldsymbol{s}}) = f(\boldsymbol{x}, \hat{\boldsymbol{s}}), \tag{1}$$

where ∇ is the surface tangential gradient and $f(\boldsymbol{x}, \hat{\boldsymbol{s}})$ is an internal source [13]. The material or acoustic parameters, such as wave speed, density and damping may vary across Ω, and are taken to be piecewise constant in the present formulation. We let $\hat{\boldsymbol{n}}(\boldsymbol{x})$ denote the outward unit normal at $\boldsymbol{x} \in \Gamma$, then for all incoming directions satisfying $\hat{\boldsymbol{s}} \cdot \hat{\boldsymbol{n}} < 0$, we apply a specular reflection boundary condition of the form

$$u(\boldsymbol{x}, \hat{\boldsymbol{s}}) = u_0(\boldsymbol{x}, \hat{\boldsymbol{s}}) + u(\boldsymbol{x},\, \hat{\boldsymbol{s}} - 2\,(\hat{\boldsymbol{s}} \cdot \hat{\boldsymbol{n}})\, \hat{\boldsymbol{n}}). \tag{2}$$

Here $u_0(\boldsymbol{x}, \hat{\boldsymbol{s}})$ represents a prescribed boundary emission and in the absence of boundary source we set $u_0(\boldsymbol{x}, \hat{\boldsymbol{s}}) = 0$. The fluence is the total wave energy density at each point $\boldsymbol{x}$, given by

$$\Phi(\boldsymbol{x}) = \int_{S^1} u(\boldsymbol{x}, \hat{\boldsymbol{s}})\, \mathrm{d}\hat{\boldsymbol{s}} = \int_{-\pi}^{\pi} u(\boldsymbol{x}, \hat{\boldsymbol{s}}(\theta))\, \mathrm{d}\theta, \tag{3}$$

where S^1 denotes the local unit circle of directions on a polygonal face.

3. Discretisation

To numerically solve the RTE, we discretise (1) using a DG method in space together with a discrete ordinates approximation in direction. The domain Ω is partitioned into N_h non-overlapping polygonal surface elements E_j, $j = 1, 2, \ldots, N_h$. Each element E_j has κ_j edges, denoted by $\Gamma_{i,j}$ for $i = 1, \ldots, \kappa_j$, with outward unit edge normal $\hat{\boldsymbol{n}}_{i,j}$ lying in the local tangent plane of E_j.

On each element E_j, the solution is approximated locally by $u_j \approx u$ for $j = 1, 2, \ldots, N_h$. The angular variable is expressed with respect to a local element tangential coordinate frame, and so we let $(\boldsymbol{e}_{x,j}, \boldsymbol{e}_{y,j})$ denote an orthonormal frame spanning the plane containing E_j. For an angle θ, the associated direction vector is defined by

$$\hat{\boldsymbol{s}}_j(\theta) = \cos(\theta)\boldsymbol{e}_{x,j} + \sin(\theta)\boldsymbol{e}_{y,j}, \tag{4}$$

which is tangential to the surface element and remains constant within E_j. This allows each surface element to be treated as a planar polygon.

For the numerical spatial integration, each element E_j is first enclosed in its minimal bounding box. If this box has centroid $(x_{c,j}, y_{c,j})$ and side lengths $h_{x,j}$ and $h_{y,j}$, we map it affinely onto the reference box $\widehat{B} = (-1, 1)^2$ via

$$\widehat{\boldsymbol{x}} = F_j(\boldsymbol{x}) = \left(\frac{2(x - x_{c,j})}{h_{x,j}}, \frac{2(y - y_{c,j})}{h_{y,j}} \right). \tag{5}$$

The mapped polygon $\widehat{E}_j = F_j(E_j) \subset \widehat{B}$, with edges $\widehat{\Gamma}_{i,j} = F_j(\Gamma_{i,j})$, is then used in the integration procedure introduced in [14] to evaluate the DG element and edge integrals exactly and efficiently, with $|\boldsymbol{J}_{E_j}|$ and $|\boldsymbol{J}_{\Gamma_{i,j}}|$ scaling the corresponding physical measures. To apply the directional discretisation through the discrete ordinates method, we represent the direction variable by a finite set of N_θ angles in $[-\pi, \pi)$, denoted by θ_n, where $n = 1, 2, \ldots, N_\theta$. Accordingly, for each discrete direction θ_n and for $\boldsymbol{x} \in E_j$, the local basis expansion is written in local element coordinates $\hat{\boldsymbol{x}} = (\hat{x}, \hat{y})$ as

$$u_j(\hat{\boldsymbol{x}}, \theta_n) = \sum_{\alpha_1=0}^{k} \sum_{\alpha_2=0}^{k-\alpha_1} u_{j,\alpha_1,\alpha_2}^{n}\, \tilde{P}_{\alpha_1}(\hat{x})\, \tilde{P}_{\alpha_2}(\hat{y}). \tag{6}$$

Here, $\tilde{P}_{\alpha_1}$ and $\tilde{P}_{\alpha_2}$ denote the one-dimensional orthonormal Legendre polynomials of degrees α_1 and α_2, respectively, where taking all index pairs (α_1, α_2) satisfying $\alpha_1 + \alpha_2 \le k$ yields a local polynomial space of total degree at most k. The DG weak formulation is then given by

$$\begin{aligned} &\int_{\hat{E}_j} \mu_j u_j\left(\hat{\boldsymbol{x}}, \theta_n\right) v_j\left(\hat{\boldsymbol{x}}\right) |\boldsymbol{J}_{E_j}|\, d\hat{\boldsymbol{x}} \\ &\quad - \int_{\hat{E}_j} u_j\left(\hat{\boldsymbol{x}}, \theta_n\right) \hat{\boldsymbol{s}}_j(\theta_n) \cdot \nabla v_j\left(\hat{\boldsymbol{x}}\right) |\boldsymbol{J}_{E_j}|\, d\hat{\boldsymbol{x}} \\ &\quad + \sum_{i=1}^{\kappa_j} \int_{\hat{\Gamma}_{i,j}} \gamma_{i,j}^{q,r,n}\left(\hat{\boldsymbol{x}}, \theta_n\right) v_j\left(\hat{\boldsymbol{x}}\right) |\boldsymbol{J}_{\Gamma_{i,j}}|\, d\hat{\boldsymbol{x}} \\ &\quad = \int_{\hat{E}_j} f_j\left(\hat{\boldsymbol{x}}, \theta_n\right) v_j\left(\hat{\boldsymbol{x}}\right) |\boldsymbol{J}_{E_j}|\, d\hat{\boldsymbol{x}}, \end{aligned} \tag{7}$$

for $j = 1, \ldots, N_h$, $n = 1, \ldots, N_\theta$ and where v_j denote the spatial test functions, chosen from the same local Legendre polynomial space. The quantity $\gamma_{i,j}^{q,r,n}$ is the multi-mode numerical flux through $\Gamma_{i,j}$ associated with the ordinate θ_n. The flux is defined using an upwind scheme that incorporates reflection, transmission and mode conversion at interfaces. To introduce this scheme, we let E_{j_+} denote the neighbouring element across $\Gamma_{i,j}$, $\hat{\boldsymbol{x}}_{i_+}$ be the point on the neighbouring edge corresponding to $\hat{\boldsymbol{x}} \in \hat{\Gamma}_{i,j}$, and $q, r \in \{B, L, S\}$ denote incident and outgoing wave modes, respectively. Writing $\mathcal{M} = \{B, L, S\}$ and $\eta_{i,j}(\theta) = \hat{\boldsymbol{s}}_j(\theta) \cdot \hat{\boldsymbol{n}}_{i,j}$, the multi-mode upwind flux $\gamma_{i,j}^{q,r,n}$ depends on the sign of $\eta_{i,j}(\theta_n)$. For positive $\eta_{i,j}(\theta_n)$, then θ_n is the incident direction in E_j and $\gamma_{i,j}^{q,r,n} =$

$$\eta_{i,j}(\theta_n) u_j^q(\widehat{\boldsymbol{x}}, \theta_n) + \sum_{q \in \mathcal{M}} \eta_{i,j}(\theta_R^{qr}(\theta_n))\, \mathcal{R}_{j,j_+}^{qr}(\theta_n)\, u_j^r(\widehat{\boldsymbol{x}}, \theta_R^{qr}(\theta_n)) .$$

Here, we let $\theta_R^{qr}(\theta_n)$ denote the reflection angle from edge $\Gamma_{i,j}$ in wave mode r arising from the incident direction θ_n in wave mode q. For negative $\eta_{i,j}(\theta_n)$, then θ_n is the transmitted post-scattering direction in E_j and $\gamma_{i,j}^{q,r,n} =$

$$\eta_{i,j}(\theta_n) \sum_{q \in \mathcal{M}} \mathcal{T}_{j_+,j}^{qr}\left(\theta_{T_+}^{qr}(\theta_n)\right) u_{j_+}^q\left(\widehat{\boldsymbol{x}}_{i_+}, \theta_{T_+}^{qr}(\theta_n)\right) .$$

Here, we let $\theta_{T_+}^{qr}(\theta_n)$ denote the incident direction which maps to θ_n after transmission from mode q to mode r. The corresponding local incident angles are measured relative to the interface normal as in the Snell's Law construction and the coefficients $\mathcal{R}_{j,j_+}^{qr}$ and $\mathcal{T}_{j_+,j}^{qr}$ are the associated reflected and transmitted power flux ratios obtained from the Langley–Heron plate-junction scattering matrix [15]–[18]. For single mode acoustic waves, the indices q, r are not necessary and the coefficients $\mathcal{R}_{j,j_+}$ and $\mathcal{T}_{j_+,j}$ are given by the Fresnel equations.

The source contribution is incorporated through the prescribed boundary radiance u_0 appearing in (2). After discretisation, we therefore set $f_j = 0$ in (7) and prescribe excitation on the appropriate boundary edges through the DG flux term, which in practice is projected onto the local DG basis and added to the right-hand side of the assembled system.

For an internal point source located at $\boldsymbol{x}_0 \in E_p$, the singular source is difficult to represent directly using the spatial polynomial basis functions. Instead, it is replaced by an equivalent boundary emission on the boundary of the source-containing element E_p and its neighbouring elements, again using the boundary radiance term u_0. Here, the material is assumed to be homogeneous across E_p and its neighbouring elements, so the wave speeds are constant and the transmission coefficient is taken to be unity. More general reflected and transmitted source contributions could be incorporated here, if required, using the same scattering framework as for the interface fluxes. At a boundary point $\boldsymbol{x} \in \Gamma_{i,p^+}$ along the i^{th} edge of E_{p^+} connected to E_p along edge i, the point source contribution is given by

$$u_0(\boldsymbol{x}, \theta) = \frac{\exp\left(-\mu_p \|\boldsymbol{x} - \boldsymbol{x}_0\|\right)}{2\pi \|\boldsymbol{x} - \boldsymbol{x}_0\|} \delta\left(\theta - \theta_0(\boldsymbol{x})\right), \quad (8)$$

where μ_p is the damping coefficient in E_p, and $\theta_0(\boldsymbol{x})$ is the direction from the source point $\boldsymbol{x}_0$ to the boundary point $\boldsymbol{x}$. The fluence inside E_p is then supplemented by the corresponding direct Green's-function contribution, while all subsequent propagation, reflection and transmission are handled through the DG edge fluxes.

After assembling the volume, flux and source contributions, the DG–DO discretisation gives the global linear system

$$\boldsymbol{A}\boldsymbol{u} = \boldsymbol{v}, \quad (9)$$

where $\boldsymbol{u}$ contains the unknown expansion coefficients over all elements, basis functions, modes and ordinates. Once $\boldsymbol{u}$ has been computed, the fluence is recovered by summing the directional radiance over the discrete ordinates. For each mode $q \in \{B, L, S\}$, the modal fluence is approximated at $\boldsymbol{x} \in E_j$ via

$$\Phi_j^q(\boldsymbol{x}) \approx \frac{2\pi}{N_\theta} \sum_{n=1}^{N_\theta} \sum_{\alpha_1=0}^{k} \sum_{\alpha_2=0}^{k-\alpha_1} u_{j,\alpha_1,\alpha_2}^{q,n} \tilde{P}_{\alpha_1}(\hat{x}) \tilde{P}_{\alpha_2}(\hat{y}). \quad (10)$$

The bending, longitudinal and shear fluences in the element E_j are therefore obtained as Φ_j^B, Φ_j^L and Φ_j^S, respectively, and for the acoustic case we can simply omit the index q as before.

4. Numerical results

We present a preliminary numerical test designed to assess the behaviour of the proposed DG–DO formulation on a simple curved surface. We consider a point source on a sphere, allowing comparison with an established geodesic flow benchmark including an exact solution from the literature [17]. Note that we assume pure wave transmission across the curved surface, and do not incorporate curvature induced reflection phenomena [19].

Letting φ denote the polar angle measured from the source location, then the exact fluence takes the form

$$\Phi_{\mathrm{sol}}(\varphi) = \frac{C \exp(-\mu\varphi)}{(1 - \exp(-2\pi\mu)) \sin\varphi}, \quad (11)$$

where μ is the damping coefficient and C is a source normalisation constant. This benchmark was used in previous literature [17] where the authors also modelled the transport of phase-space energy densities on triangulated surfaces using discrete flow mapping. Here, we use the same analytic solution to test our DG–DO formulation for the fluence compared with the geodesic solution in equation (11). We also fix $k = 0$ and vary the number of surface elements N_h and angular ordinates N_θ, since the error from approximating the curved surface by a triangulated surface limits the benefit of increasing k for this example.

Table 1: Errors for the spherical point-source benchmark test with fixed polynomial degree $k = 0$.

N_h	$N_\theta = 256$	$N_\theta = 512$	$N_\theta = 1024$
320	1.02e-1	1.04e-1	1.01e-1
1280	6.47e-2	5.80e-2	5.96e-2
5120	4.26e-2	4.05e-2	3.94e-2
20480	3.11e-2	2.93e-2	2.76e-2

In line with [17], the resulting errors from the centroids of the elements are averaged over the upper hemisphere and reported in Table 1. Figure 1 compares a

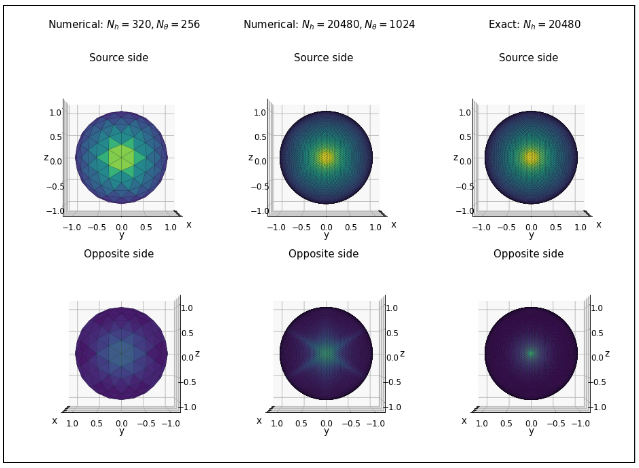

Figure 1: Approximate and reference fluence on the triangulated sphere for the point-source geodesic transport benchmark. The exact solution is represented on a triangulation with $N_h = 20480$ elements, consistent with the mesh used for the most accurate numerical solution.

coarse DG–DO solution ($N_h = 320, N_\theta = 256$), a more accurate DG–DO solution ($N_h = 20480, N_\theta = 1024$), and the corresponding reference fluence plotted on a log scale. The DG–DO errors decrease under mesh refinement and, less significantly, by increasing N_θ. In comparison with the discrete flow mapping results reported in [17], we find that the error on the finest mesh is reduced from 5.12×10^{-2} in [17] to 2.76×10^{-2} here. Also, from Figure 1, it can be observed that the computed solution converges towards the exact geodesic solution, with the refocusing near the antipodal point becoming sharper as the mesh is refined and more discrete ordinates are used.

5. Conclusion

We have presented a numerical framework for modelling high-frequency acoustic and vibrational energy in complex built-up structures. The approach is based on the radiative transfer equation without inscattering, discretised using a discontinuous Galerkin method in space and a discrete ordinates approximation in direction. This formulation facilitates the propagation of wave energy densities over unstructured polygonal surface meshes, making it suitable for shells, multi-plate surfaces and built-up acoustic systems. The formulation can incorporate multi-material interfaces and plate junctions, with reflection, transmission and mode-conversion conditions via the upwind flux using the Langley–Heron scattering coefficients. Preliminary validation examples demonstrate the potential of the method for curved-surface ray density transport problems.

6. Acknowledgments

R. Lockett gratefully acknowledges a PhD studentship from Nottingham Trent University.

References

[1] V. Cervený, *Seismic Ray Theory*. Cambridge, UK: Cambridge University Press, 2001, vol. 110.

[2] L. Cremer and M. Heckl, *Structure-borne sound: structural vibrations and sound radiation at audio frequencies*. Springer Science & Business Media, 2013.

[3] H. Kuttruff, *Room Acoustics*, 6th ed. Boca Raton, United States: CRC Press, 2016.

[4] B. Engquist and O. Runborg, “Computational high frequency wave propagation”, *Acta Numerica*, vol. 12, pp. 181–266, 2003.

[5] G. Tanner, “Dynamical energy analysis—determining wave energy distributions in vibro-acoustical structures in the high-frequency regime”, *J. Sound Vib.*, vol. 320, no. 4–5, pp. 1023–1038, 2009.

[6] J. Rowbottom and D. J. Chappell, “On hybrid convolution quadrature approaches for modeling time-domain wave problems with broadband frequency content”, *Int. J. Numer. Methods Eng.*, vol. 122, no. 24, pp. 7581–7608, 2021.

[7] R. Lyon, “Statistical analysis of power injection and response in structures and rooms”, *J. Acoust. Soc. Amer.*, vol. 45, pp. 545–565, 1969.

[8] R. Lyon and R. DeJong, *Theory and Application of Statistical Energy Analysis*. Boston: Butterworth-Heinemann, 1995.

[9] T. Lafont, N. Totaro, and A. Le Bot, “Review of statistical energy analysis hypotheses in vibroacoustics”, *Proc. Roy. Soc. A*, vol. 470, no. 2162, 2014, 20130515.

[10] M. C. Gutzwiller, *Chaos in Classical and Quantum Mechanics*. Springer, 1990.

[11] G. Tanner and N. Søndergaard, “Wave chaos in acoustics and elasticity”, *J. Phys. A: Math. Theor.*, vol. 40, no. 50, R443–R509, 2007.

[12] D. Chappell, J. J. Crofts, M. Richter, and G. Tanner, “A direction preserving discretization for computing phase-space densities”, *SIAM J. Sci. Comput.*, vol. 43, no. 4, B884–B906, 2021.

[13] S. Chandrasekhar, *Radiative Transfer*. New York, United States: Dover Publications Inc, 1960.

[14] P. F. Antonietti, P. Houston, and G. Pennesi, “Fast numerical integration on polytopic meshes with applications to discontinuous Galerkin finite element methods”, *J. Sci. Comput.*, vol. 77, no. 3, pp. 1339–1370, 2018.

[15] R. S. Langley and K. H. Heron, “Elastic wave transmission through plate/beam junctions”, *J. Sound Vib.*, vol. 143, no. 2, pp. 241–253, 1990.

[16] N. Aimakov, G. Tanner, and D. Chronopoulos, "Transmission and reflection of waves at structural junctions connecting thin orthotropic plates", *Wave Motion*, vol. 102, 2021, 102716.

[17] D. J. Chappell, G. Tanner, D. Löchel, and N. Søndergaard, "Discrete flow mapping: Transport of phase space densities on triangulated surfaces", *Proc. Roy. Soc. A*, vol. 469, no. 2155, 2013, 20130153.

[18] C. Brewer, S. C. Creagh, and G. Tanner, "Elastodynamics on graphs—wave propagation on networks of plates", *J. Phys. A: Math. Theor.*, vol. 51, no. 44, 2018, 445101.

[19] N. Søndergaard and D. J. Chappell, "Ray and wave scattering in smoothly curved thin shell cylindrical ridges", *J. Sound Vib.*, vol. 377, pp. 155–168, 2016.